

advances.sciencemag.org/cgi/content/full/6/38/eaba3126/DC1

Supplementary Materials for

Cavefish brain atlases reveal functional and anatomical convergence across independently evolved populations

James B. Jaggard, Evan Lloyd, Anders Yuiska, Adam Patch, Yaouen Fily, Johanna E. Kowalko, Lior Appelbaum, Erik R. Duboue, Alex C. Keene*

*Corresponding author. Email: keenea@fau.edu

Published 16 September 2020, *Sci. Adv.* **6**, eaba3126 (2020)
DOI: [10.1126/sciadv.aba3126](https://doi.org/10.1126/sciadv.aba3126)

The PDF file includes:

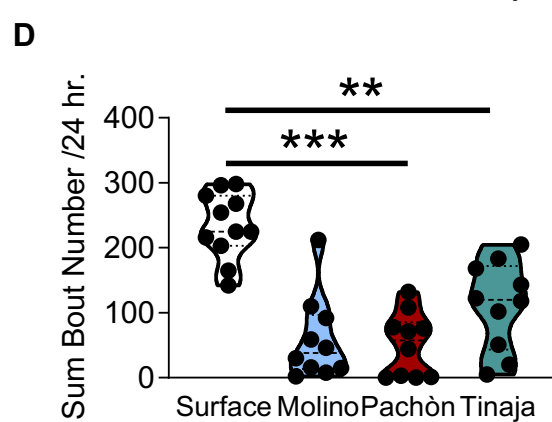
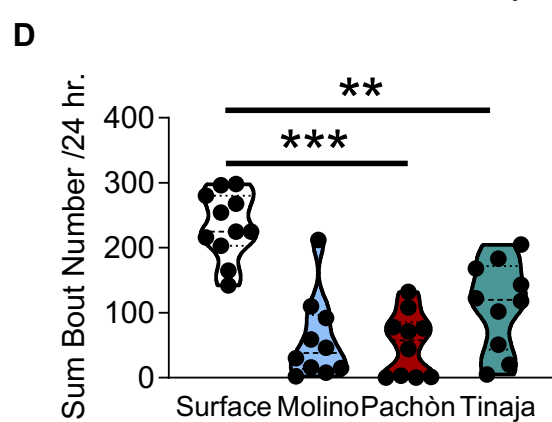
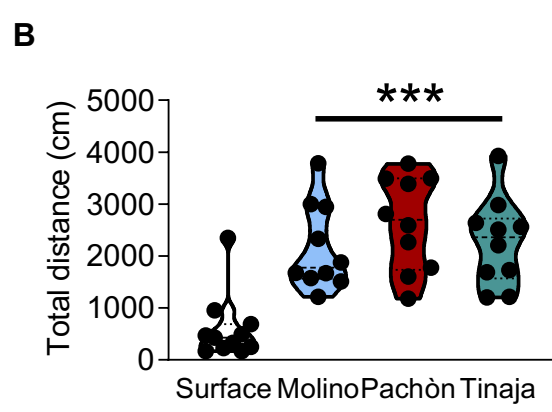
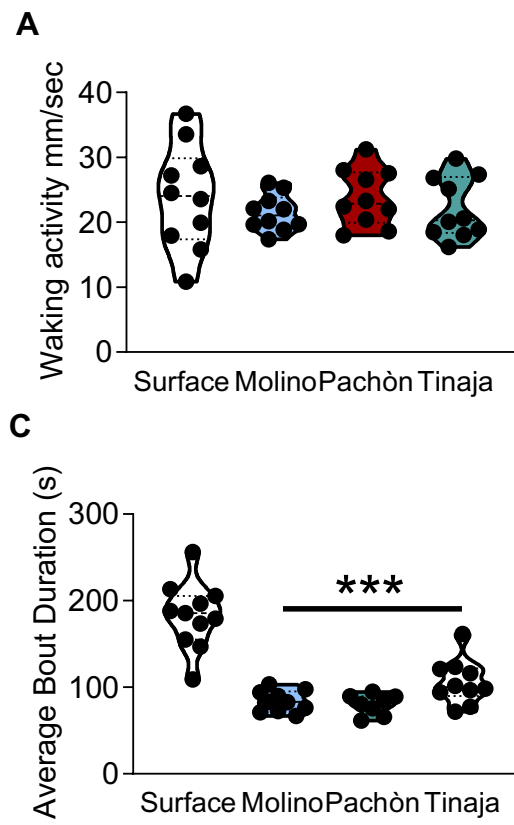
Figs. S1 to S15
Legends for movies S1 to S7
Legends for tables S1 to S5

Other Supplementary Material for this manuscript includes the following:

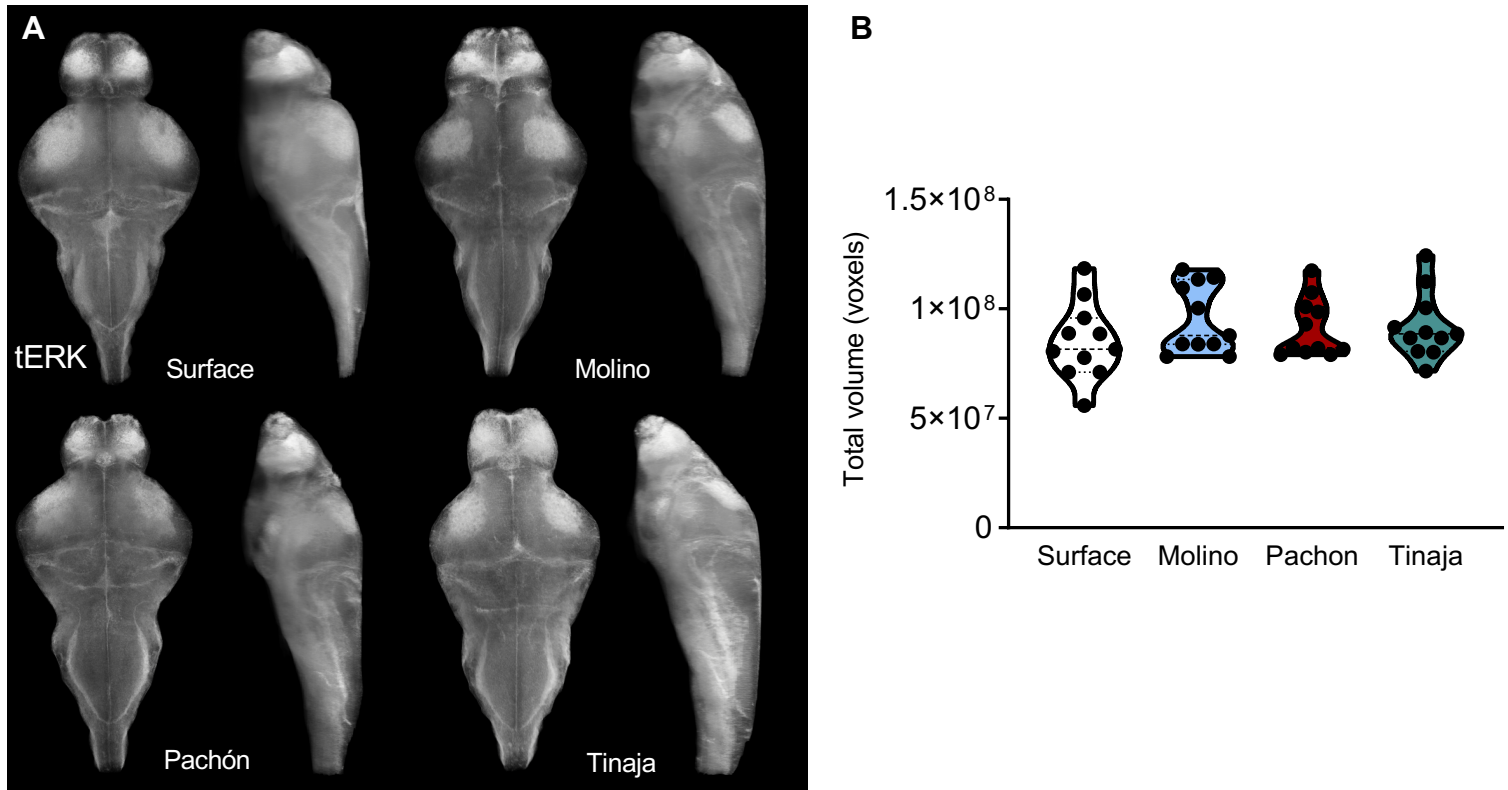
(available at advances.sciencemag.org/cgi/content/full/6/38/eaba3126/DC1)

Movies S1 to S7
Tables S1 to S5

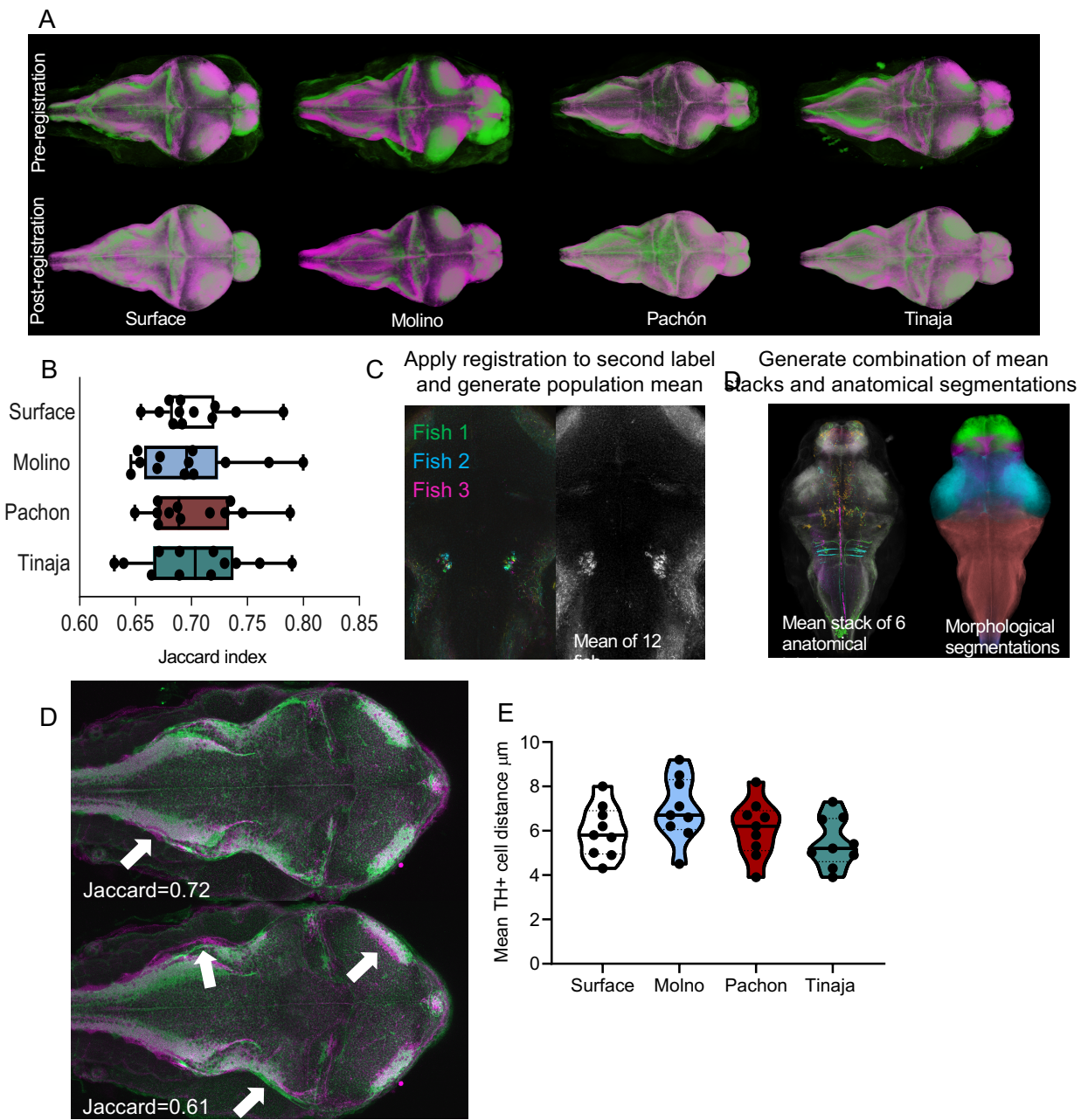
Supplemental figure 1. Quantification of sleep architecture and feeding behavior



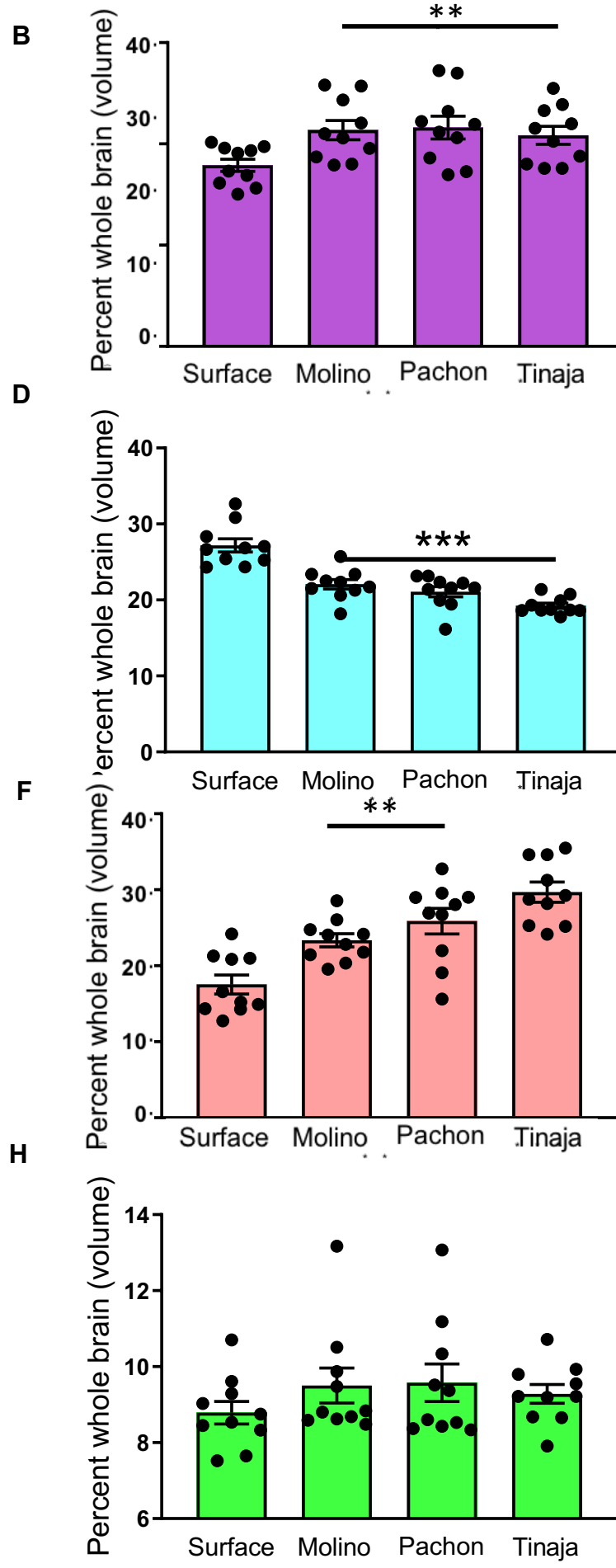
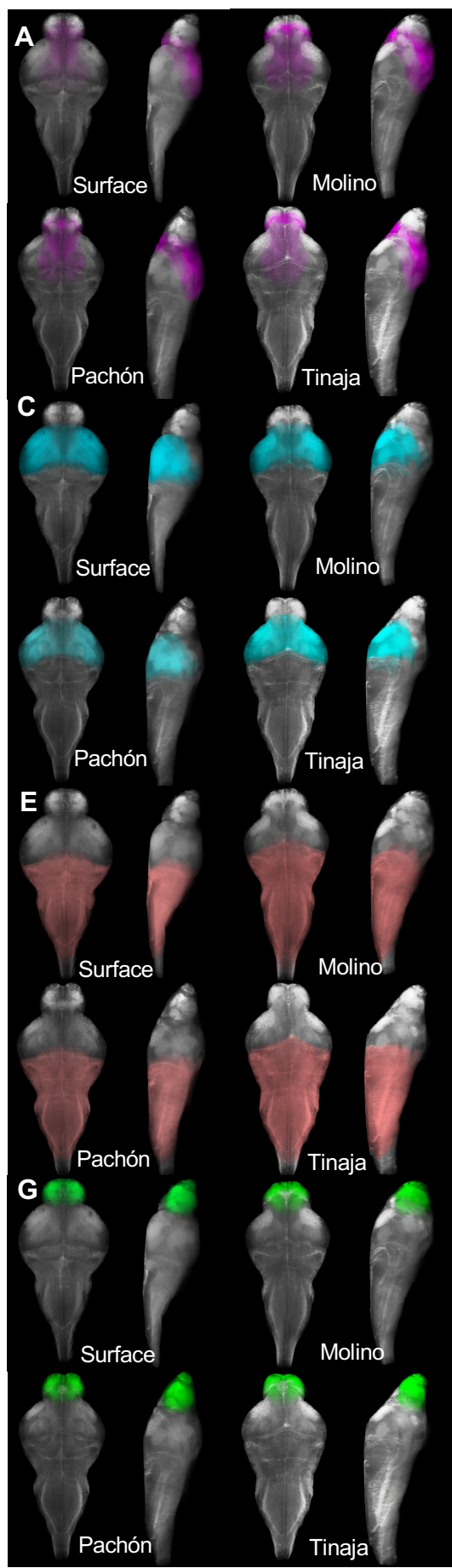
Supplemental figure 2. Whole brain size is not significantly differ among populations of *A. mexicanus*



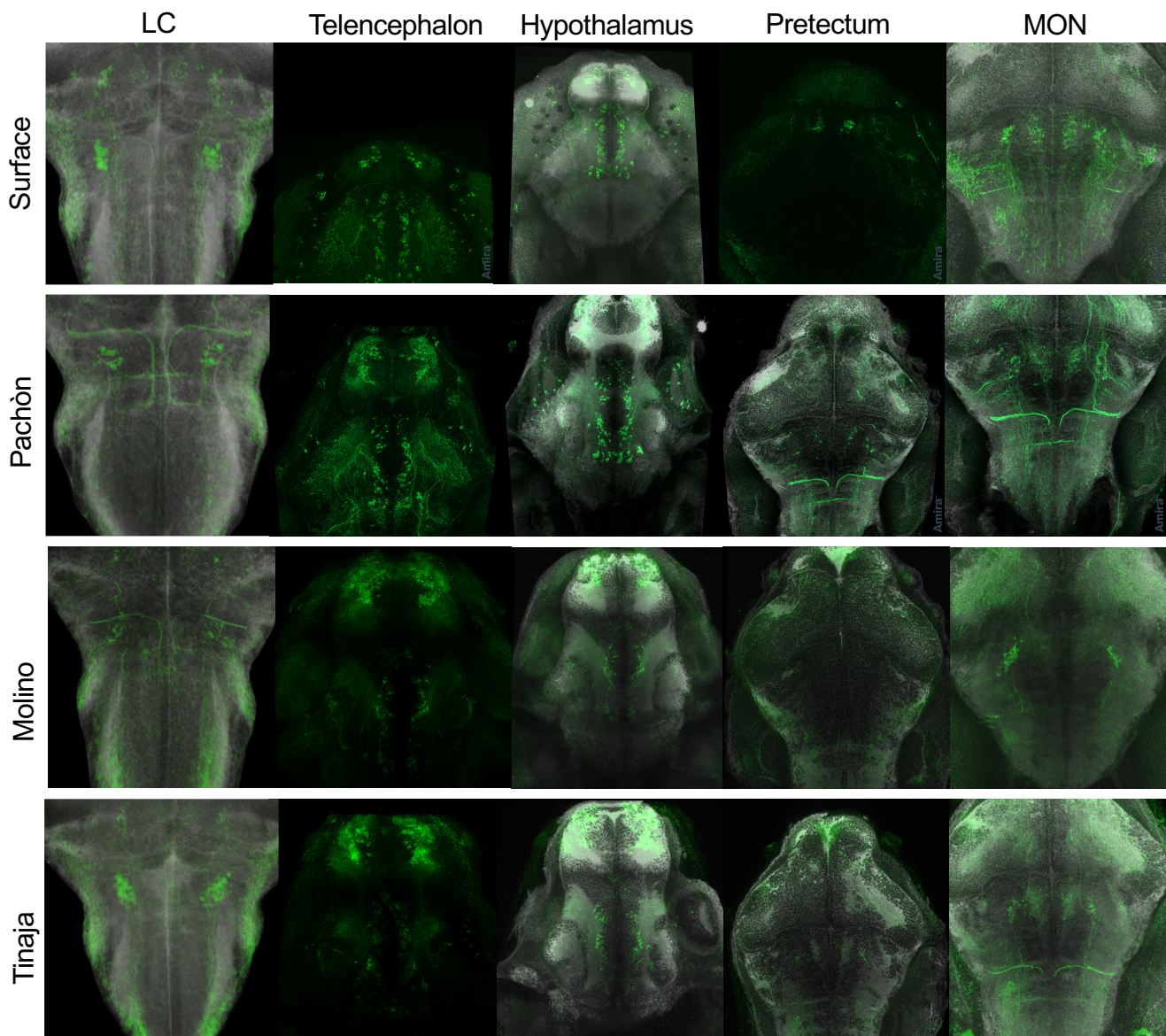
Supplemental figure 3. Image registration in *A. mexicanus* brains



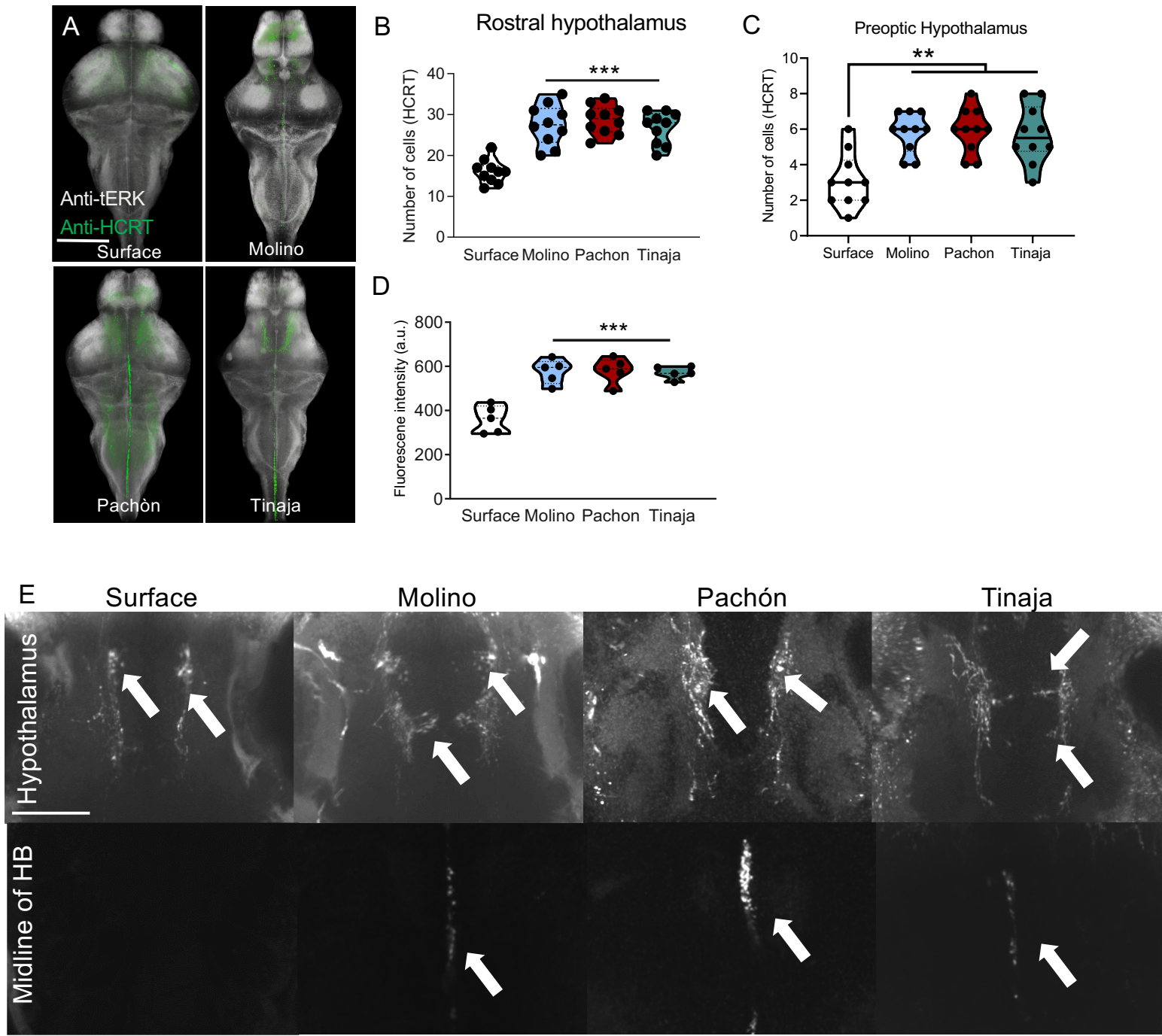
Supplemental figure 4. Evolution of neural developmental regions



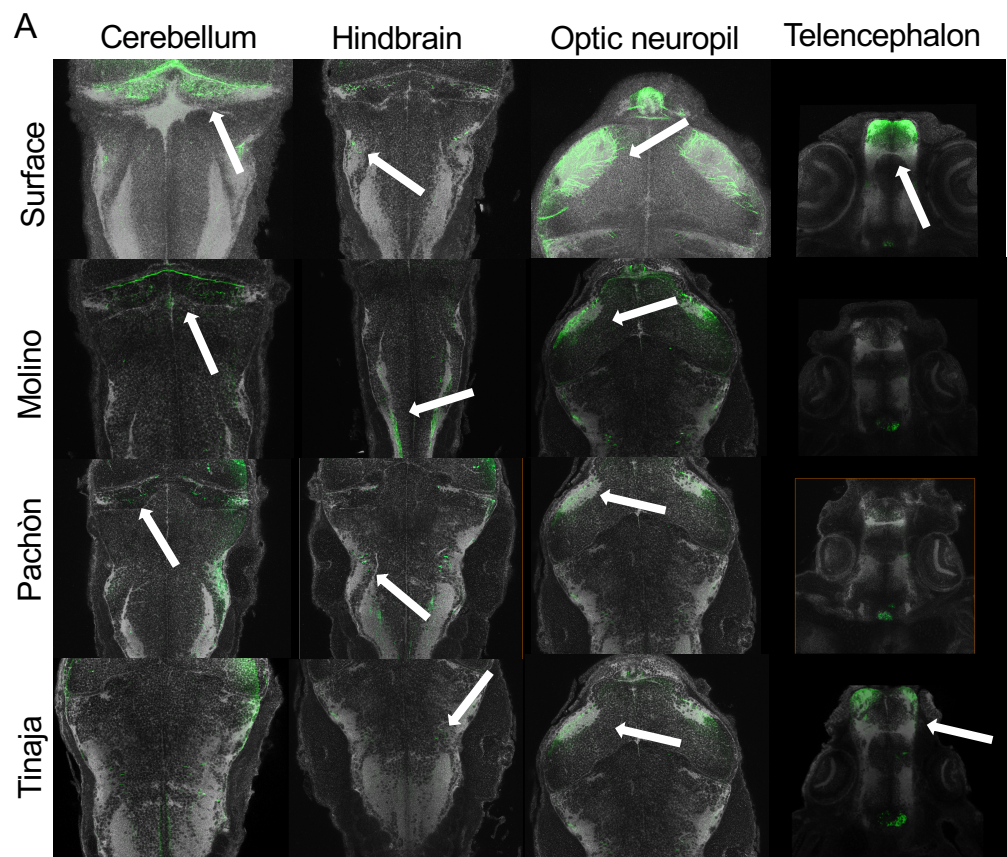
Supplemental figure 5. Neuroanatomical characterization of TH circuitry



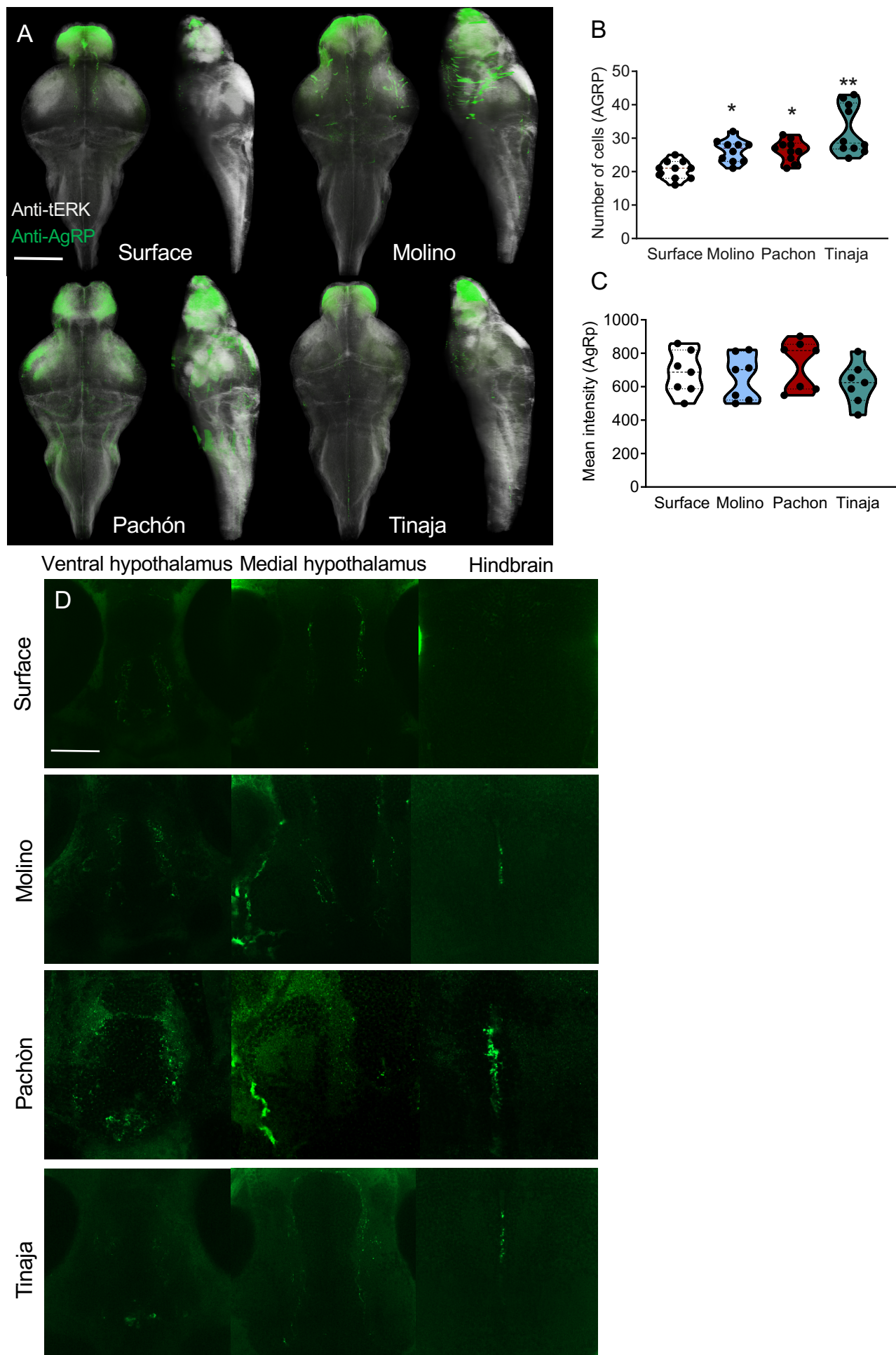
Supplemental figure 6: Convergent evolution of HCRT circuitry



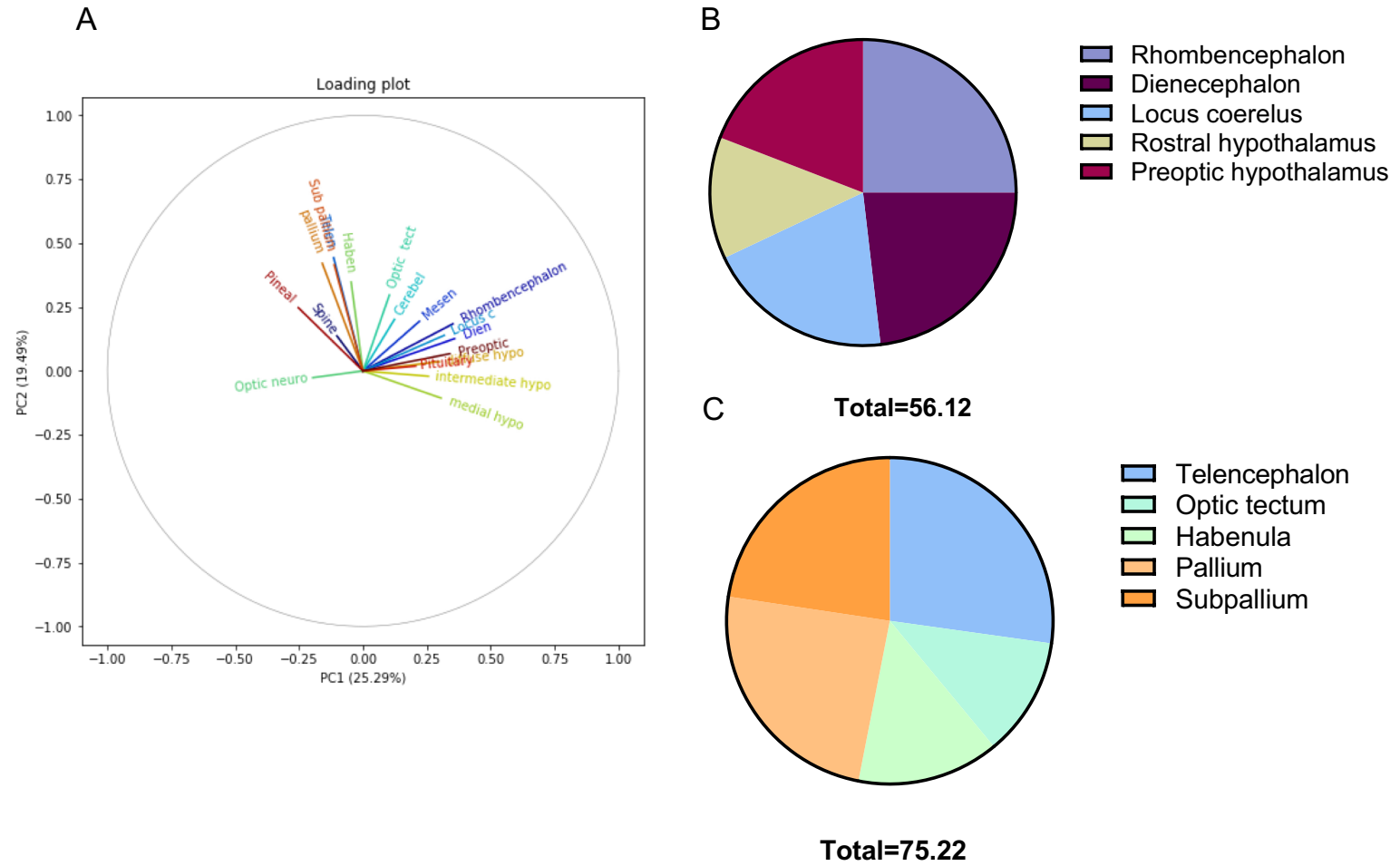
Supplemental figure 7. Reduced number of α -MSH neurons in cavefish



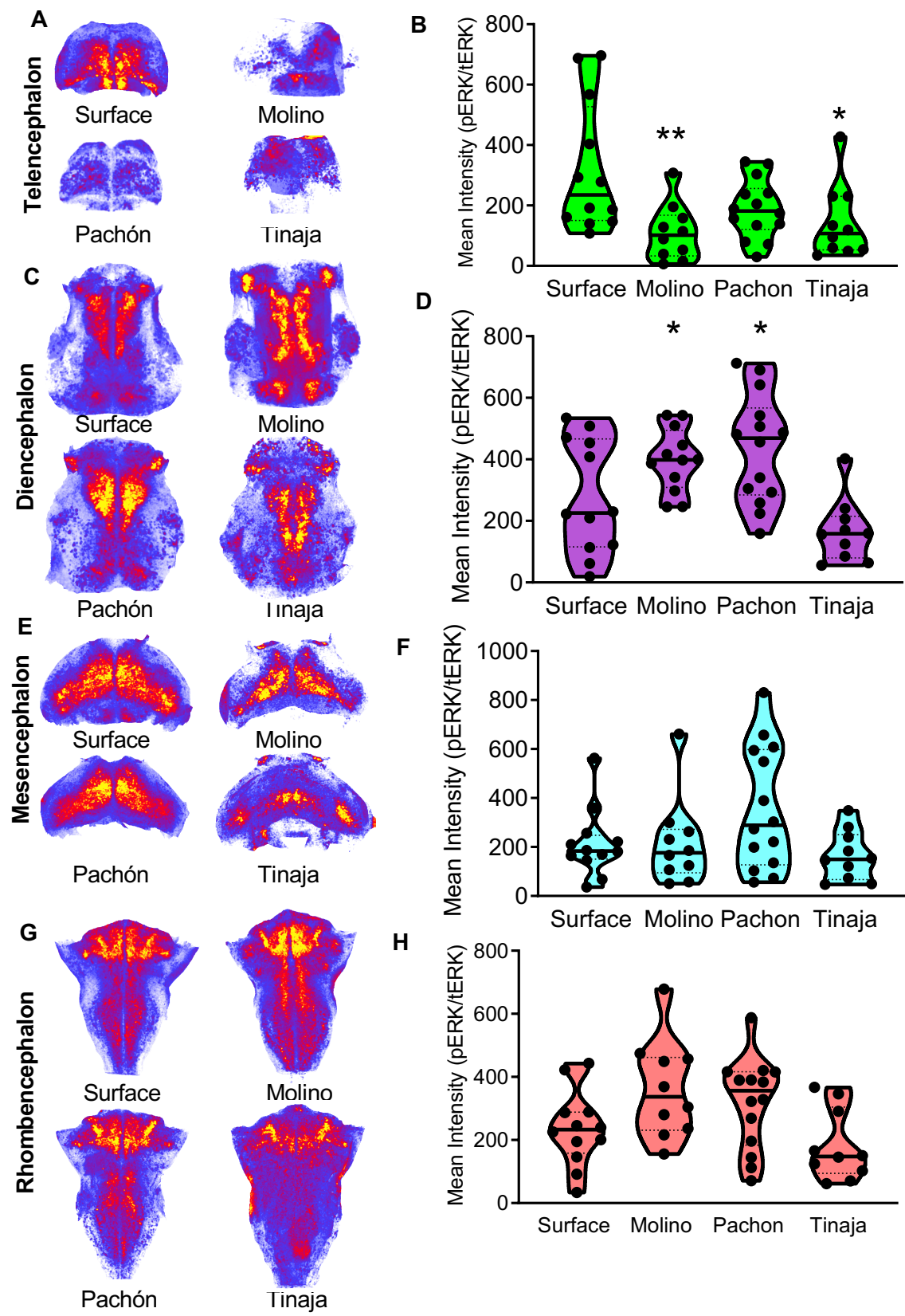
Supplemental figure 8. Increased number of AgRP neurons in cavefish



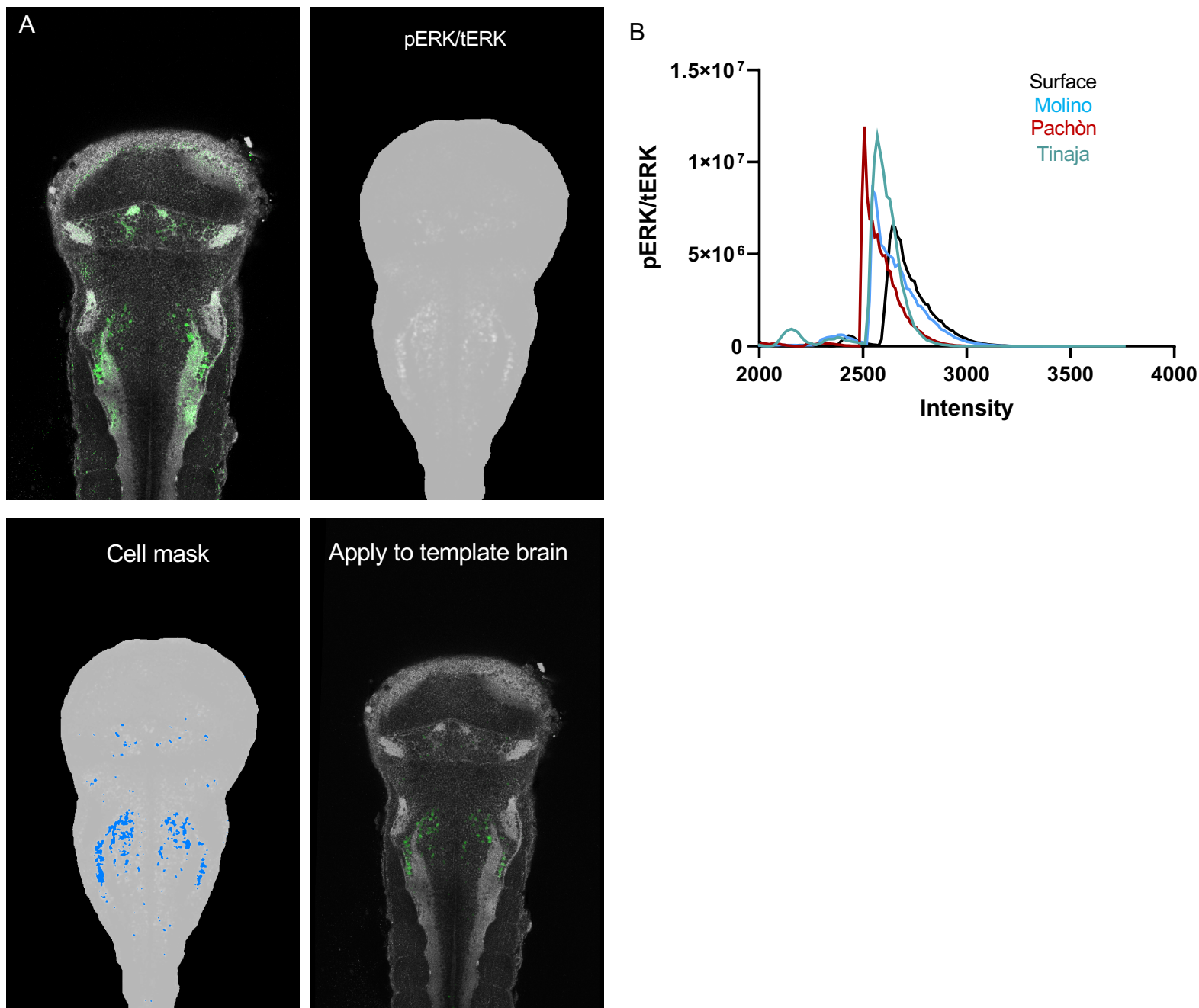
Supplemental figure 9: Variable analysis for anatomical contributions to PC1 and PC2



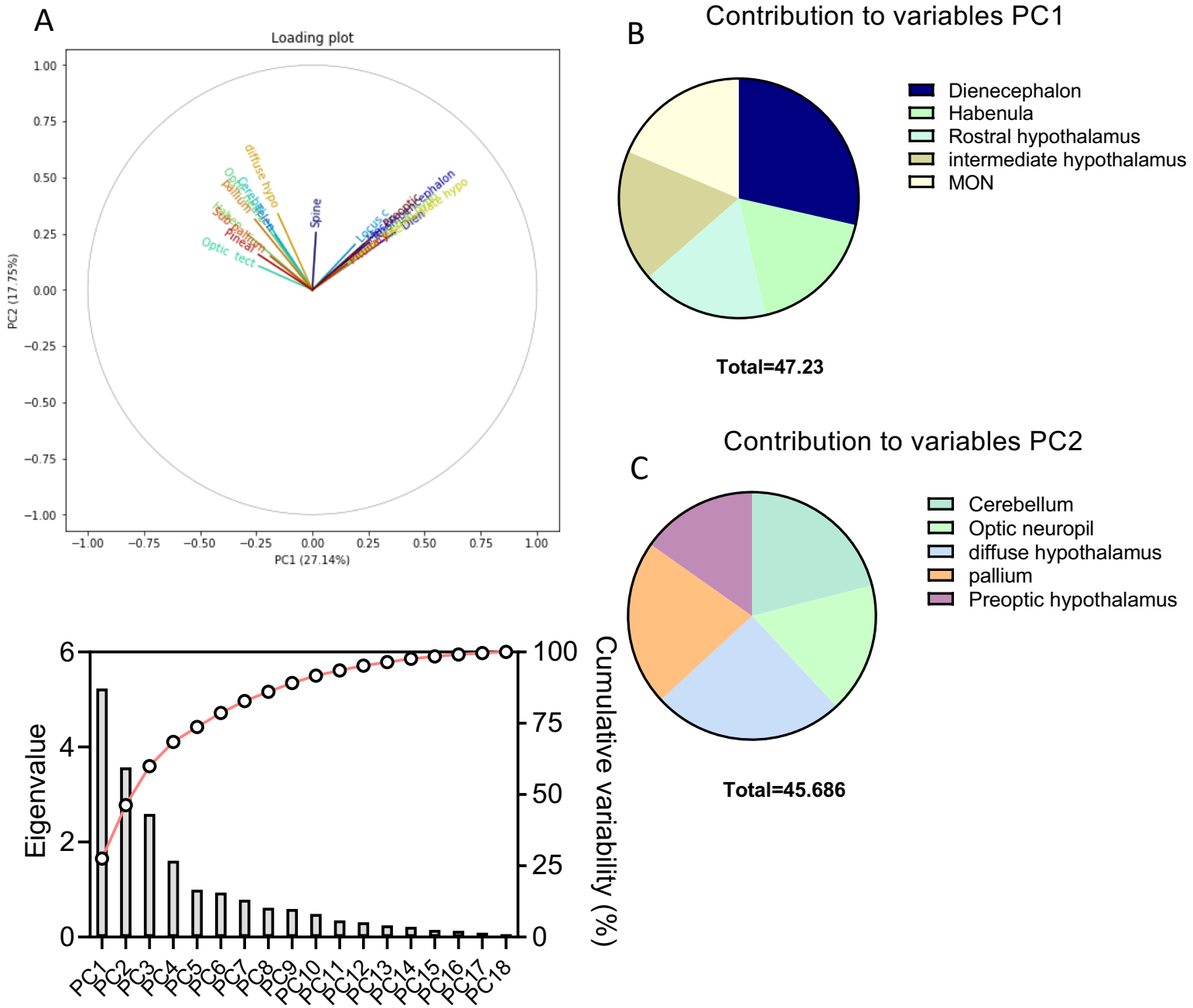
Supplemental figure 10. Quantification of neural activity in developmental divisions of the brain



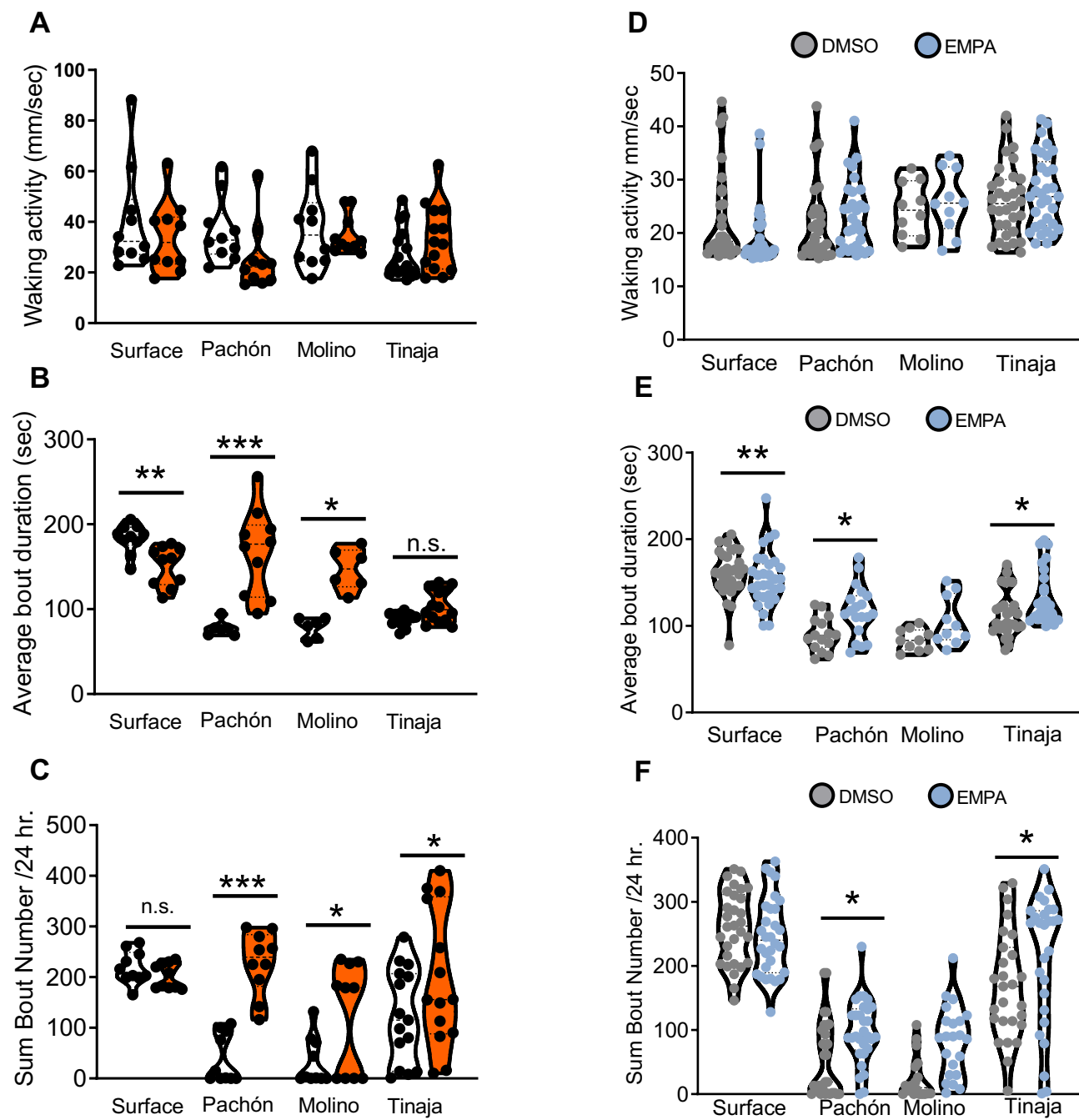
Supplemental figure 11. Pipeline for pERK quantification of whole-brain activity mapping



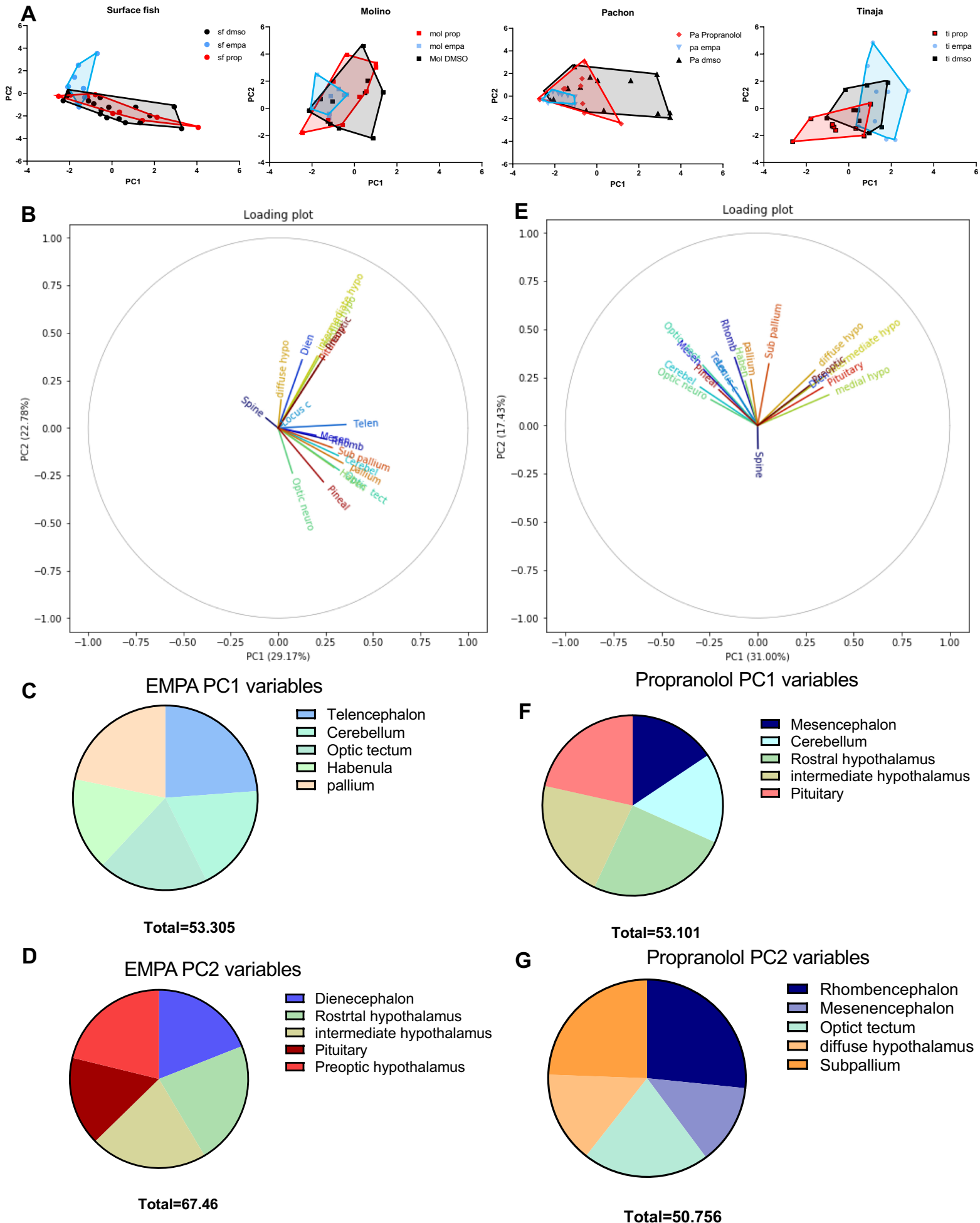
Supplemental figure 12. PCA and variable analysis for feeding brain activity



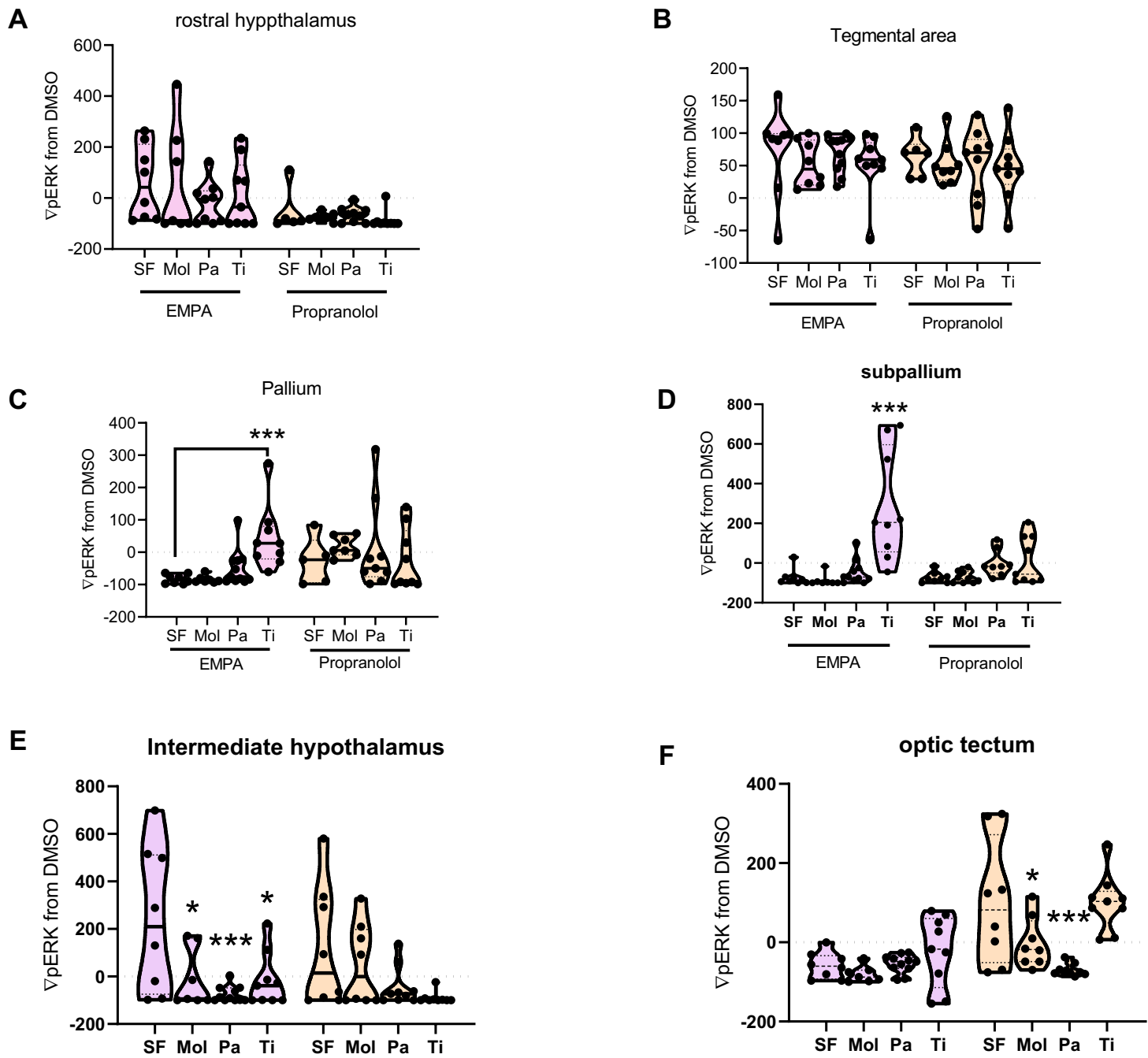
Supplemental 13. Sleep architecture for Propranolol and EMPA treatments



Supplemental figure 14. PCA and Variable analysis for drug treatments



Supplemental figure 15: Regions with sleep-associated changes in neural activity



Supplementary Information

Supplemental figure 1: Quantification of sleep architecture in individual A. mexicanus populations. **A.** Waking activity did not vary significantly among the four populations of *A. mexicanus* (1-way ANOVA, $F=0.518$, $P=0.672$; Molino, $p>0.61$, Pachón, $p>0.99$, Tinaja, $p>0.81$). **B.** All cave populations have converged upon significant increases in total locomotion per 24 hours relative to surface fish (1-way ANOVA, $F=13.45$, $P<0.001$; Molino, Pachón, Tinaja, $p<0.001$). **C.** Average sleep bout duration was significantly reduced in all populations of cavefish compared to surface fish (1-way ANOVA, $F=35.82$, $P<0.001$; Molino, Pachón, Tinaja, $p<0.001$). **D.** Sum of bout number was significantly reduced in all cave populations relative to surface fish (1-way ANOVA, $F=22.01$, $p<0.001$; Molino, Pachón, Tinaja, $p<0.001$).

Supplemental figure 2: Whole brain size does not differ among populations of A. mexicanus. **A.** Whole-brain confocal scans of tERK antibody signal. Each population is depicted in dorsal (left) and sagittal (right) aspects. Scale bar denotes 300 μm . **B.** Quantification of whole-brain scans revealed no significant difference among populations in brain size (1-way ANOVA, $F=0.869$, $P=0.46$; Molino, $p>0.69$, Pachón, $p>0.27$, Tinaja, $p>0.59$).

Supplemental figure 3: Image registration in A. mexicanus brains. **A.** Examples of brains before (top) and after (bottom) alignment to the template brain (green) and transformed brain (green) for four populations of *A. mexicanus*. **B.** Jaccard image similarity analysis detected no differences in registration quality across populations. (1-way ANOVA, $F=0.02$, $P=0.99$). **C.** Registrations applied to an anatomical label (anti-TH). Left panel shows TH staining in locus coeruleus for three fish, each colored differently. Right panel shows population average of TH+ expression in locus coeruleus from 10 fish. **D.** Registered labels were combined together to create the standard brain and applied to morphological neuroanatomy. Means of six different labels and five different segmented areas are shown. **E.** Mean distance error of registered TH+ cells in the locus coeruleus was quantified for all populations. Error did not differ significantly across populations (1-way ANOVA, $F=2.27$, $P=0.09$).

Supplemental figure 4: Evolution of neural developmental regions. **A.** Volumetric projection of diencephalon (magenta). **B.** Convergence of expanded diencephalon in cavefish populations (1-way ANOVA, $F=3.56$, $P=0.02$; Molino, $p<0.02$, Pachón, $p<0.01$, Tinaja, $p<0.04$). **C.** Volumetric projection of mesencephalon (cyan). **D.** Reduction of mesencephalon in all cavefish populations (1-way ANOVA, $F=26.72$, $p<0.001$; Molino, Pachón, Tinaja, $p<0.001$). **E.** Volumetric projection of rhombencephalon (red). **F.** Rhombencephalon is expanded in cavefish relative to surface fish (1-way ANOVA, $F=15.15$, $p<0.001$; Molino, $p<0.01$, Pachón, $p<0.001$, Tinaja, $p<0.001$). **G.** Volumetric projection of telencephalon (green). **H.** Telencephalon size did not significantly differ among *A. mexicanus* populations (1-way ANOVA, $F=0.845$, $P=0.47$; Molino, $p>0.42$ Pachón, $p>0.35$ Tinaja, $p>0.68$). Scale bar for all images is 300 μm .

Supplemental figure 5: Neuroanatomical characterization of the TH circuitry. Close-up views of cell clusters within nuclei across the brain in surface, Molino, Pachón, and

Tinaja. Left, locus coeruleus; second from left, telencephalon; middle, hypothalamus; second from right, pretectum; right, medial octavolateralis nucleus.

Supplemental figure 6: Convergent evolution of HCRT in cave-dwelling *A. mexicanus*. **A.** Whole-brain volumetric projections of tERK (white) and hypocretin (green). Scale bar, 300 μ m. **B.** Quantification of hypocretin cells in rostral zone of the hypothalamus in 6-day old fish reveals a convergence of enhanced HCRT in all cave populations relative to surface fish (1-way ANOVA, $F=22.5$, $P<0.01$; Molino, Pachón, Tinaja, $p<0.001$). **C.** Preoptic hypothalamus HCRT cluster was significantly larger in cave-adapted populations than in surface fish (1-way ANOVA, $F=9.21$, $P<0.001$; Molino, Pachón, Tinaja, $p<0.001$). **D.** Fluorescence intensity per HCRT cell was higher in cavefish in both rostral zone of the hypothalamus preoptic hypothalamus (1-way ANOVA, $F=20.69$, $P<0.001$; Molino, Pachon, Tinaja, $p<0.001$).

Supplemental figure 7: Reduced number of α -MSH neurons in cavefish. Single-plane views of confocal scans showing tERK (white) and α -MSH staining across the brain of 6-dpf *A. mexicanus*. Left panel: the cerebellum exhibits greater immunoreactivity in surface fish than in all populations of cavefish. Second from left: hindbrain expression was largely the same across all populations of *A. mexicanus*. Second from right: optic neuropil was highly immunoreactive in surface fish, with lower expression in all cave populations. Right: telencephalon was highly immunoreactive to MSH in surface and Tinaja, but not in Molino or Pachón.

Supplemental figure 8: Increased number of AgRP neurons in cavefish. **A.** Whole-brain volumetric projections of tERK (white) and AgRP (green). Scale bar, 300 μ m. **B.** Quantification of AgRP+ cells in the pituitary complex reveals a convergence on higher numbers of cells in all populations of cavefish relative to surface fish (1-way ANOVA $F=11.18$, $P<0.001$; Molino, $p<0.02$, Pachón, $p<0.02$, Tinaja, $p<0.001$). **C.** Fluorescence intensity did not differ among populations of cavefish or surface fish (1-way ANOVA, $F=0.88$, $P=0.46$; Molino, $p>0.82$, Pachón, $p>0.70$, Tinaja, $p>0.97$). **D.** Single-plane confocal views of AgRP expression in the ventral hypothalamus, showing immunoreactive fibers in the hypothalamic and forebrain bundles (left). In the medial plane of the hypothalamus, signal was intense in the diffuse nucleus of the hypothalamus in Molino and Pachón, but not in surface or Tinaja (middle). All cave populations exhibited intense IR expression at the midline through the hindbrain. No such expression was observed in surface fish (right).

Supplemental figure 9: Variable analysis for anatomical contributions to PC1 and PC2. **A.** Variable vectors revealed a spread of regions affecting both PC1 along the x-axis and PC2 along the y-axis. **B.** Top five variables that contribute to PC1, including rhombencephalon, diencephalon, locus coeruleus, rostral zone of the hypothalamus, and preoptic region of the hypothalamus. These five regions contribute to 55.09% of the variability in PC1. **C.** Top regions for variation in PC2, including the telencephalon, optic tectum, habenula, pallium, and subpallium. Together, these regions contribute 66.31% of the variation in PC2.

Supplemental figure 10: Quantification of neural activity in developmental divisions of the brain. **A.** Max intensity projection of pERK activity in the telencephalon. **B.** Reduced forebrain activity in cave-adapted populations (1-way ANOVA, $F=4.78$, $P=0.005'$ Molino,

$p<0.003$, Pachón, $p=0.06$, Tinaja, $p<0.01$) **C.** Max intensity projection of diencephalon pERK activity. **D.** Quantification of pERK in diencephalon (1-way ANOVA, $F=7.51$, $P<0.001$; Molino, $p<0.03$, Pachón, $p<0.03$, Tinaja, $p=0.2$). **E.** Max intensity projections of neural activity measured by pERK in the mesencephalon. **F.** Quantification of mesencephalon neural activity (1-way ANOVA, $F=2.61$, $P=0.063$; Molino, $p>0.13$, Pachón, $p>0.99$, Tinaja, $p>0.86$) **G.** Rhombencephalon pERK activity by max projection. **H.** Quantification of neural activity in hindbrain (1-way ANOVA, $F=3.82$, $P>0.01$; Molino, $p>0.28$, Pachón, $p>0.08$, Tinaja, $p>0.69$). Scale bar denotes 200 μm for all images.

Supplemental figure 11: Pipeline for pERK quantification for whole-brain activity mapping. **A.** Top left panel: single plane confocal scan with tERK (white) and pERK (green). Top right panel: pERK/tERK with brain mask applied after registration to the template brain. Bottom left: application of cell mask; blue represents cells that were kept for the activity map that were statistically significantly different from background. Bottom right: Activity map (green) applied to the template brain (white). **B.** pERK/tERK ratio histograms for all basal free-swimming fish. Cell mask was generated for each individual fish by applying a 5% cutoff from the peak of the histogram.

Supplemental figure 12: PCA and variable analysis for feeding brain activity. **A.** Loading plot analysis shows variable vectors with a spread of regions affecting both PC1 along the x-axis and PC2 along the y-axis.. **B.** PC1. **C.** PC2

Supplemental figure 13: Sleep architecture for Propranolol and EMPA treatments. **A.** Waking activity is not altered by drug treatments (2-way ANOVA, $F=1.43$, $P>0.2$) **B.** Average bout duration was altered by EMPA and Propranolol treatment in *A. mexicanus* (2-way ANOVA, $F=20.04$, $P<0.001$; EMPA: Surface, $p>0.82$, Molino, $p>0.02$, Pachón, $p>0.04$, Tinaja, $p>0.03$. Propranolol: Surface, Molino, $p>0.03$, Pachón, $p>0.001$, Tinaja, $p>0.12$) **C.** Total sleep bout number was altered by both EMPA and Propranolol treatments (2-way ANOVA, $F=48.77$, $P<0.001$; EMPA, Surface, $p>0.85$ Molino, $p>0.04$ Pachón, $p>0.02$ Tinaja, $p>0.07$. Propranolol: Surface, $p>0.94$ Molino, $p>0.02$ Pachón, >0.001 Tinaja, $p>0.01$).

Supplemental figure 14: PCA and Variable analysis for anatomical contributions to PC1 and PC2 during drug treatments. **A.** PCA of all population comparing EMPA and Propranolol drug treatments with DMSO controls **B.** Loading plot for EMPA treatment **C.** Top anatomical regions from variables in PC1 for EMPA treatment **D.** Top neuroanatomical regions for PC2 in EMPA treatment **E.** Loading plot for Propranolol treatment. **F.** Top neuroanatomical regions for PC1 in Propranolol treatment **G.** Top neuroanatomical regions for PC2 during Propranolol treatment.

Supplemental figure 15: Regions with sleep-associated changes in neural activity. **A.** Quantification of change in pERK activity from DMSO to drug treatment in the rostral zone of the hypothalamus (2-way ANOVA, $F=2.24$, $P<0.04$; EMPA: Molino, $p>0.99$, Pachón, $p>0.61$, Tinaja, $p>0.94$. Propranolol: Molino, $p>0.99$, Pachón, $p>0.99$, Tinaja, $p>0.99$) **B.** Change in pERK activity from DMSO to drug treatment in the tegmental area (2-way ANOVA, $F=0.38$, $P>0.91$; EMPA: Molino, $p>0.93$, Pachón, $p>0.99$, Tinaja, $p>0.92$. Propranolol: Molino, $p>0.99$, Pachón, $p>0.99$, Tinaja, $p>0.98$ **C.** Quantification of change in pERK activity from DMSO to drug treatment in the Pallium (2-way ANOVA, $F=2.24$, $P<0.04$; EMPA: Molino, $p>0.99$, Pachón, $p>0.61$, Tinaja, $p>0.94$. Propranolol: Molino, $p>0.99$, Pachón, $p>0.99$, Tinaja, $p>0.99$). **D.** Quantification of change in pERK activity from DMSO to drug treatment in the subpallium (2-way ANOVA, $F=10.01$, $P<0.001$;

EMPA: Molino, $p>0.99$, Pachón, $p>0.99$, Tinaja, $p<0.001$. Propranolol: Molino, $p>0.99$, Pachón, $p>0.76$, Tinaja, $p>0.55$) **E.** Quantification of change in pERK activity from DMSO to drug treatment in the intermediate hypothalamus (2-way ANOVA, $F=4.00$, $P<0.001$; EMPA: Molino, $p<0.02$, Pachón, $p>0.001$, Tinaja, $p>0.01$. Propranolol: Molino, $p>0.95$, Pachón, $p>0.24$, Tinaja, $p>0.05$). **F.** Quantification of change in pERK activity from DMSO to drug treatment in the optic tectum (2-way ANOVA, $F=8.55$, $P<0.001$; EMPA: Molino, $p>0.99$, Pachón, $p>0.99$, Tinaja, $p>0.89$. Propranolol: Molino, $p>0.04$, Pachón, $p<0.001$, Tinaja, $p>0.99$).

Supplemental Video 1: Representative neuroanatomical segmentations through whole brain.

Supplemental Video 2: Three-dimensional reconstructions of neuroanatomical segmentations for surface, Molino, Pachón, and Tinaja fish. tERK antibody was used to visualize neural tissue. Colors denote anatomical regions, which were labelled computationally.

Supplemental Video 3: Example stacks showing transformed brains (magenta) and template brains (green).

Supplemental video 4: Standard brain for each population of *A. mexicanus*. Neural tissue is visualized with tERK antibody (white). Anti-TH (green) anti-HCRT (magenta) anti-AgRP (red) anti-MSH (cyan). Average pERK activity during basal conditions in orange.

Supplemental video 5: Basal whole brain activity throughout whole brain. pERK activity is shown in green, registered onto template brains (white).

Supplemental video 6: Whole-brain activity during non-fed and fed conditions. pERK neural activity for non-fed (green) and fed (magenta) aligned to reference brains in tERK (white) for each population.

Supplemental Video 7: Whole-brain activity during drug-induced sleep. Neural activity associated waking DMSO (green) and sleeping EMPA (magenta) and Propranolol (yellow)

Supplemental Table 1. Statistics related to figure 1. Includes normality tests and variance tests for behavior, as well as normality and variance tests for segmented regions of morphological data with sizes and statistics. Blue cells contain behavioral statistics (related to Fig1B-C). Orange cells contain statistics for developmental region morphology related to Fig1H. Green cells contain statistics for subnuclei, related to Fig 1M.

Supplemental Table 2: Antibodies used with concentrations and part numbers

Supplemental Table 3: PCA of Basal pERK/tERK neural activity. First tab contains raw data, second tab contains PCA analysis. Includes correlation matrix, eigenvalues, correlations between brain regions and PCs, variable contribution to each PC, and individual factor score for each PC.

Supplemental Table 4: PCA of Neural activity measured with pERK/tERK activity during feeding. First tab contains raw data, second tab contains PCA. Includes correlation matrix, eigenvalues, correlations between brain regions and PCs, variable contribution to each PC, and individual factor score for each PC.

Supplemental Table 5: pERK quantification in all segmented brain regions during drug treatments.